



Structural and Functional Analysis of Surface Film on Li Anode in Vinylene Carbonate-Containing Electrolyte

Hitoshi Ota,^{a,*} Yuuichi Sakata,^a Yumiko Otake,^a Kunihisa Shima,^a Makoto Ue,^{a,*} and Jun-ichi Yamaki^{b,*}

^aMitsubishi Chemical Group Science and Technology Research Center, Incorporated, Ibaraki 300-0332, Japan

^bInstitute for Materials Chemistry and Engineering, Kyushu University, Kasuga 816-8580, Japan

The lithium cycling efficiencies of the lithium anode in the ethylene carbonate (EC)-based electrolytes were improved by adding vinylene carbonate (VC) to the electrolyte. We analyzed the surface films of deposited lithium on a nickel substrate in a VC-containing electrolyte with scanning electron microscopy, Fourier transform infrared spectroscopy, two-dimensional nuclear magnetic resonance, gel permeation chromatography, and X-ray photoelectron spectroscopy. The corresponding surface films comprise various polymeric species including poly-(vinylene carbonate) [poly-(VC)], oligomeric VC, and a ring-opened polymer of VC. Furthermore, the surface film of carbon double bonds (C = C-O) and lithium carboxylate (RCOOLi) as reduction products of VC were formed on deposited lithium. These structures of the surface film on the lithium anode were similar to those on the graphite anode. At elevated temperatures, the VC-containing electrolyte led to the formation of surface films comprising poly-(VC). The VC-derived polymeric surface film, which exhibited gel-like morphology, could prevent the deleterious reaction which occurs between deposited lithium and the electrolyte, resulting in an enhanced lithium cycling efficiency.

© 2004 The Electrochemical Society. [DOI: 10.1149/1.1798411] All rights reserved.

Manuscript submitted September 8, 2003; revised manuscript April 29, 2004. Available electronically October 4, 2004.

A large number of studies have been conducted on rechargeable batteries which use lithium metal anodes, because of lithium's high theoretical specific capacity (3860 Ah kg^{-1}). The main areas of research have focused primarily on investigating several key aspects including low lithium cycling efficiency, the occurrence of deleterious dendrite-like lithium deposits on the anode, and general safety concerns.¹ These problems have been widely believed to result from the reaction of freshly deposited lithium with the electrolyte components.

The use of LiAsF_6 as a solute has sparked considerable interest due to its excellent lithium cycling efficiency.²⁻⁶ However, the toxicity of LiAsF_6 limits the practical application of this material as a suitable electrolyte. The use of imide salts such as $\text{LiN}(\text{SO}_2\text{C}_2\text{F}_5)_2$ (LiBETI) have been proposed to yield higher lithium cycling efficiencies and a more enhanced cycling performance.⁷⁻⁹ Further, the use of lithium organoborate with a salicylic ligand has also demonstrated a certain success in improving the lithium cycling performance in the ethylene carbonate (EC) and dimethoxyethane (DME) solvent system.¹⁰ The ether compounds such as 2-methyltetrahydrofuran (2-MeTHF),²⁻⁵ 1,3-dioxolane (DN),⁶ tetrahydropyran (THP),⁸ and 1,3-dioxane (DOX),⁹ which have good reductive stability, are effective solvents for the lithium metal rechargeable batteries. Another key area of research generating much interest concerns the incorporation of additives into the electrolyte. Many attempts have proposed that the addition of inorganic compounds,¹¹⁻¹⁶ organic compounds,^{11,17,18} surfactants,¹⁹⁻²¹ and gaseous compounds²²⁻²⁵ to the electrolyte improves the lithium cycling efficiency and cycling performance of the lithium metal rechargeable batteries. Inorganic additives such as Al_3 result in a Li-Al alloy interface with a high conductivity.¹³ The addition of hydrofluoric acid (HF) to electrolytes results in a smoothly deposited lithium morphology on the anode surface and a much enhanced cycling performance.^{14-16,26} The presence of dissolved CO_2 within the electrolyte has also proven effective for enhancing the cycling performance of lithium batteries,²²⁻²⁵ forming a Li_2CO_3 film on the lithium anode.²³ The incorporation of organic additives such as 2-methylfuran within the electrolyte also results in an enhanced cycling performance due to the surface film formation on reaction with the deposited lithium.¹⁷ The addition of aromatic additives such as benzene and toluene induces an isolation effect with the electrolyte

since they adhere to the lithium metal anode, resulting in an improved lithium cycling efficiency.¹⁷ Fluoroethylene carbonate has also been proposed as an additive for improving the lithium cycling performance of the lithium anode.²⁸ Additives such as ethylene sulfite and VC, which are known to prevent the decomposition of propylene carbonate (PC) on graphite anodes, have so far shown no improvements in the cycling performance.¹⁸ The addition of VC to the electrolytes has been proposed in order to improve the performance of lithium batteries which use graphite anodes.²⁷ It is known that treating the electrodes to a stacked pressure also influences the lithium cycling performance of the lithium anode.²⁸ Moreover, the lithium cycling efficiencies are influenced by the temperature conditions during deposition and dissolution.²⁹⁻³²

Recently, we reported that the lithium cycling efficiency for deposited lithium on nickel substrates in VC-containing electrolytes can be improved if the electrodes are pressurized.³³ Lithium cycling efficiencies in EC + dimethyl carbonate (DMC) (1:1) electrolytes containing either LiPF_6 , LiBF_4 , $\text{LiN}(\text{SO}_2\text{CF}_3)_2$ (LiTFSI), or LiBETI at 25 and 50°C increased following the addition of VC. This is in stark contrast to the same reactions at lower temperatures (0°C), where the deposited lithium exhibits a thick dendrite-like morphology on the anode surface, causing a high film resistance, and ultimately a decrease in the lithium cycling efficiency. At elevated temperatures (50°C), the surface films are much thinner than those formed at 0°C, and exhibit a particulate morphology.

Generally, the electrochemical behavior of lithium electrodes in organic electrolytes is controlled by the surface chemistry of the lithium metal. The reduction of electrolyte components on the lithium surface results in the formation of insoluble species, which influence the overall effectiveness of the lithium batteries. Consequently, surface characterization of the lithium electrodes plays an important role in determining the main factors which effect the cycling efficiency. Aurbach *et al.* have argued that the solid electrolyte interphase (SEI) layers on lithium in an EC-based electrolyte consist of $(\text{CH}_2\text{OCO}_2\text{Li})_2$ as the dominant constituent by Fourier transform infrared (FTIR) spectroscopy.³⁴ Moreover, their group investigated whether various inorganic and organic lithium compounds, such as lithium carbonate (Li_2CO_3), lithium oxide (Li_2O), lithium hydride (LiOH), lithium fluoride (LiF), alkyl carbonate species (ROCO_2Li) to reduce alkyl carbonate, alkoxy species (ROLi) to reduce esters, and alkyl carboxylate species (RCO_2Li) to esters, are detected in the surface film. Kanamura *et al.* reported that SEI layers deposited on lithium in a nonaqueous electrolyte by adding fluoric acid (HF) consist of an $\text{LiF}/\text{Li}_2\text{O}$ bilayer, based on X-ray photoelectron spectroscopy.

* Electrochemical Society Active Member.

^z E-mail: ota.hitoshi@mp.m-kagaku.co.jp

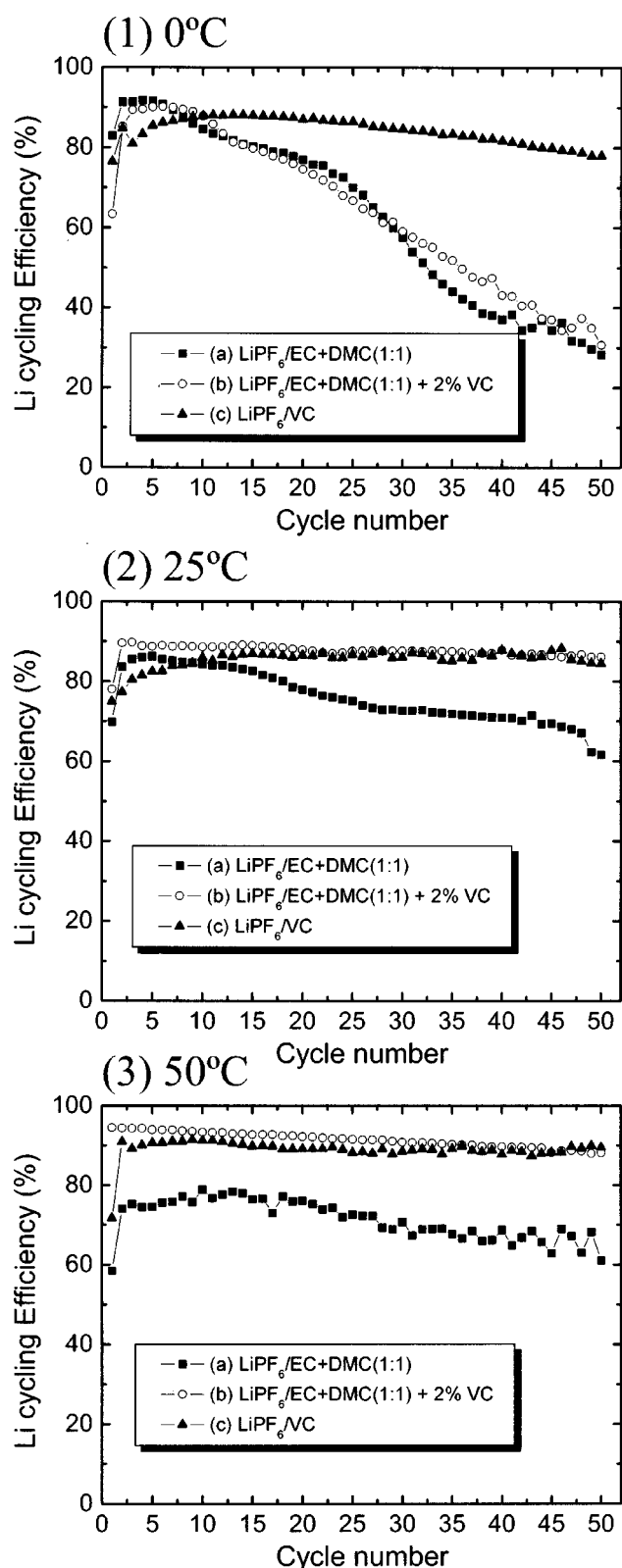


Figure 1. Lithium cycling efficiencies for deposition and dissolution of lithium on Ni anode in (a) $1 \text{ mol dm}^{-3} \text{ LiPF}_6/\text{EC} + \text{DMC} (1:1)$, (b) $1 \text{ mol dm}^{-3} \text{ LiPF}_6/\text{EC} + \text{DMC} (1:1) + 2 \text{ wt } \% \text{ VC}$, and (c) $1 \text{ mol dm}^{-3} \text{ LiPF}_6/\text{VC}$ at various temperatures: (1) 0, (2) 25, and (3) 50°C.

copy (XPS).¹⁴⁻¹⁶ Recently, Ota *et al.* reported the organic surface films of deposited lithium on nickel substrates in the EC-THF electrolyte consist of lithium etoxides, lithium ethylene dicarbonate

$(\text{CH}_2\text{OCO}_2\text{Li})_2$, polyethylene oxide, and lithium ethylene dicarbonate containing an oxyethylene, based on two-dimensional nuclear magnetic resonance (2D NMR) spectroscopy.³⁵

In this study, we examined the structure and function of the surface films of deposited lithium on nickel substrates in the VC-containing electrolytes by scanning electron microscopy (SEM), FTIR, two-dimensional nuclear magnetic resonance (2D NMR), gel permeation chromatography (GPC), XPS, and temperature programmed desorption or decomposition-mass spectrometry (TPD-MS).

Experimental

Evaluation of lithium cycling efficiency and sample preparation.—The lithium cycling efficiency was evaluated using sealed coin-type cells with a charge-discharge apparatus (Nagano, BTS2004W) in a constant temperature oven maintained within $\pm 0.5^\circ\text{C}$. Charging and discharging were performed at 0, 25, and 50°C. The cells were prepared in an argon glove box. The working electrode was a 1.25 cm diam nickel foil (99.7%, Nilaco). The counter electrode and the reference electrode were made of lithium foil (>99.8%, Honjo Metal) with the same diameter. The electrolytes (Sol-Rite, Mitsubishi Chemical Corp.) were EC + DMC solvent (volume ratio of 1:1) containing $1 \text{ mol dm}^{-3} \text{ LiPF}_6$, as the solute. The vinylene carbonate (VC, Mitsubishi Chemical Corp.) content was 2 wt %. Additionally, VC-containing $1 \text{ mol dm}^{-3} \text{ LiPF}_6$ was used as the electrolyte. The VC contained no stabilizer. The water content in the electrolytes was analyzed to be <10 ppm by Karl-Fischer titration. The electrodes were separated by a polyethylene separator and held together by a stainless steel disk with a spring. Cells were assembled in an argon-filled glove box. The lithium deposition and dissolution current density were 0.6 mA/cm^2 , and lithium of 0.5 C/cm^2 was deposited. The cut-off potential was 1.5 V for the lithium dissolution. The cell was dismantled in the argon-filled glove box. The analytical samples were transported to instruments using inactive transfer vessels. All analytical samples, except those for XPS, were prepared at 0.6 mA/cm^2 (current density) and 0.5 C/cm^2 (plating charge). Samples for XPS analysis were prepared at 0.6 mA/cm^2 (current density) and 1.6 C/cm^2 (plating charge).

Evolved gas analysis.—The evolved gas in the cell was analyzed by gas chromatography (GC). Separation of the degradation products in the evolved gases was obtained using a plot-Q column and molecular sieve column. The GC column was programmed at the constant temperature of 70°C.

Microscopic observations.—After the tenth charge-discharge test, the working electrode was removed from the coin cell and rinsed by highly purified dimethoxyethane (F-DME, battery grade, Mitsubishi Chemical Corp.) with a water content below 5 ppm in the argon-filled glove box in order to remove the electrolyte. After drying under vacuum for 30 min at room temperature, the working electrode was moved for surface observation by using a transfer vessel. Cross-sectional morphology of lithium on the working electrode was observed by using SEM (JEOL, JEM-6300F).

Nuclear magnetic resonance spectroscopy (NMR).—All NMR spectra were obtained using a NMR spectrometer (JEOL JNM-GSX400) operating at 400 MHz for the ^1H nucleus and 100 MHz for the ^{13}C nucleus. The surface film of deposited lithium on the nickel substrate after the 50th deposition/dissolution cycle was extracted with dimethyl sulfoxide (DMSO)-*d*₆ in the argon-filled glove box. The dissolved solution with DMSO was used as the NMR measurement solutions. All spectra were recorded at room temperature, and DMSO was used as the internal standard. Further details may be found elsewhere.³⁵

Gel permeation chromatography (GPC).—The number and weight average molecular weights (M_n and M_w) of surface films dissolved with DMSO were determined using a GPC (TOSOH-

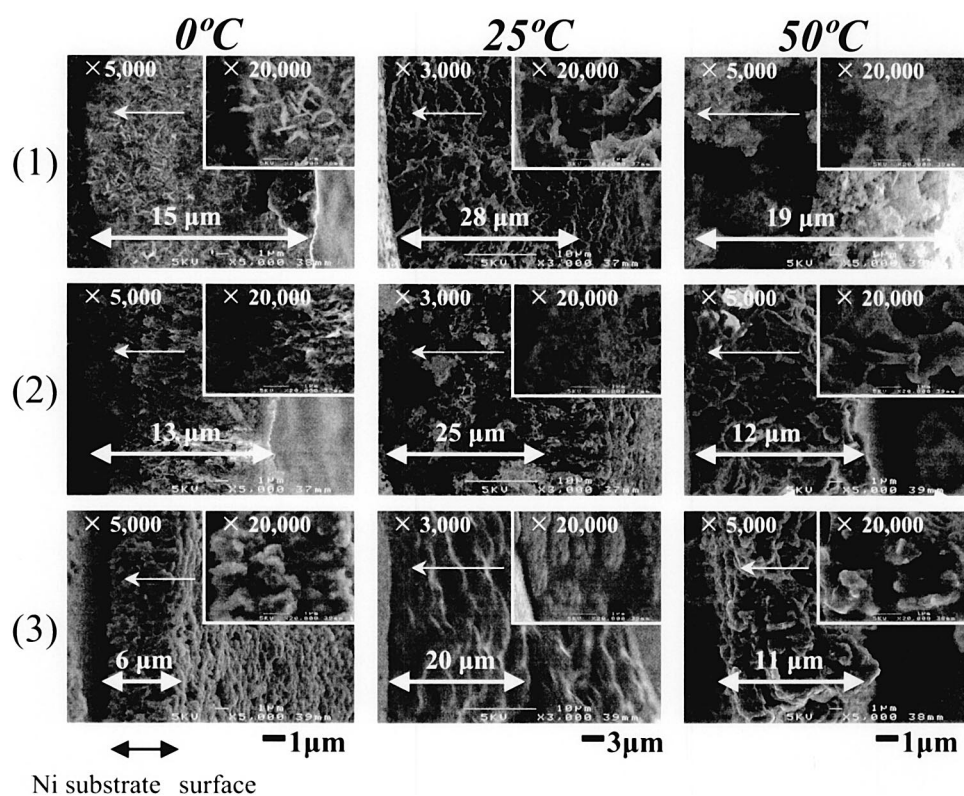


Figure 2. Cross-sectional SEM images of surface film on Ni anode in (1) 1 mol dm⁻³ LiPF₆/EC + DMC (1:1), (2) 1 mol dm⁻³ LiPF₆/EC + DMC (1:1) + 2 wt % VC, and (3) 1 mol dm⁻³ LiPF₆/VC at 0, 25, and 50°C.

HLC2000) instrument equipped with two PL gel mixed-C columns and a refractive index (RI) detector. Samples were eluted with a dimethylformamide (DMF) solution containing 10 mmol/L lithium bromide (LiBr) at a flow rate of 1.0 mL/min at 50°C. The GPC was calibrated against the following polyethylene oxide (PEO) standards (M_w 460,000; 124,700; 58,400; 29,600; 11,840; 6,450; 4,120; and 1,900).

X-ray photoelectron spectroscopy (XPS).—XPS (ULVAC-PHI5700ci) was used to obtain information about the elementary chemical state and depth profile distribution for the surface film. The surface film of deposited lithium on the nickel substrate was rinsed using F-DME. Monochromatic Al-K radiation (1486.6 eV), which operated at a power of 350 W (14 kV), was applied as the X-ray source. All XPS measurements were done on the sample after the first deposition/dissolution. Sputtering of the sample surface was performed with an argon ion gun under an accelerating voltage of 3 kV. All the samples were measured after 0, 1, 5, 15, and 45 min of Ar⁺ ion sputtering.

Fourier transform infrared spectroscopy (FTIR).—The organic components of the surface film of deposited lithium on nickel substrate after the tenth deposition/dissolution cycle were characterized by FTIR (Nicolet Magna500) equipped with a TGS detector. Spectra were obtained using a resolution of 4 cm⁻¹ and averaged over 32 scans. The measurement was carried out by the attenuated total reflectance (ATR) method. The surface film was rinsed using F-DME in the argon-filled glove box.

Temperature programmed desorption or decomposition—Mass spectrometry.—The thermal stability of the surface film of deposited lithium on the nickel substrate after the tenth deposition/dissolution cycle was evaluated by TPD-MS (ANELVA AGS-7000) equipped with a quadrupole mass spectrometer. The carrier gas was helium of 60 mL/min flow rate. The heating rate was 10°C/min. The surface film was rinsed using F-DME in the argon-filled glove box.

Results and Discussion

Lithium cycling efficiencies and cross-sectional SEM morphology studies of surface films.—Figure 1 compares the lithium cycling efficiencies for lithium deposited on a nickel substrate in the presence of three different electrolytes in LiPF₆/EC + DMC (1:1), LiPF₆/EC + DMC (1:1) + 2 wt % VC, and LiPF₆/VC at 0, 25, and 50°C. In a previous study, we observed that the cycling efficiencies of deposited lithium on a nickel substrate in an EC + DMC (1:1) electrolyte containing either LiPF₆, LiBF₄, LiTFSI, or Li-BETI at both 25 and 50°C, improved in the presence of VC when the electrodes were pressurized.³³ This was in stark contrast to the results obtained at 0°C, where the lithium cycling efficiencies showed no improvement on addition of VC. In this study, we found that the pressurized electrode cell in the LiPF₆/VC electrolyte exhibited satisfactory cycling efficiencies at low temperature. For the lithium metal anode, it is common knowledge that the coulombic efficiency is strongly dependent on the morphology of the deposited lithium.³⁶ Figure 2 shows cross-sectional SEM images of the surface film after the tenth lithium dissolution at various temperatures. These morphologies are dead lithium because SEM observations are carried out at a lithium dissolution state. In the VC and VC-free LiPF₆/EC + DMC (1:1) electrolytes at low temperature, the deposited lithium exhibits a dendrite-like morphology which is much thinner than that obtained at 25°C, resulting in a subsequent decrease in the lithium cycling efficiency (Fig. 1). The dendritic lithium can be isolated from the substrate by conducting repeated deposition and dissolution.³⁷ The isolated lithium becomes electrochemically inactive. However, the surface film increases when repeating the deposition/dissolution of lithium due to the high reactivity of isolated lithium. The dendrite-like morphology cause the formation of thicker films, although it has little or no influence on the initial lithium cycling efficiency, leading to an overall decrease in the final cycling efficiency. In the LiPF₆/VC electrolyte at low temperatures, the deposited lithium exhibits a particulate morphology, which presumably might result in an improved cycling efficiency. At higher

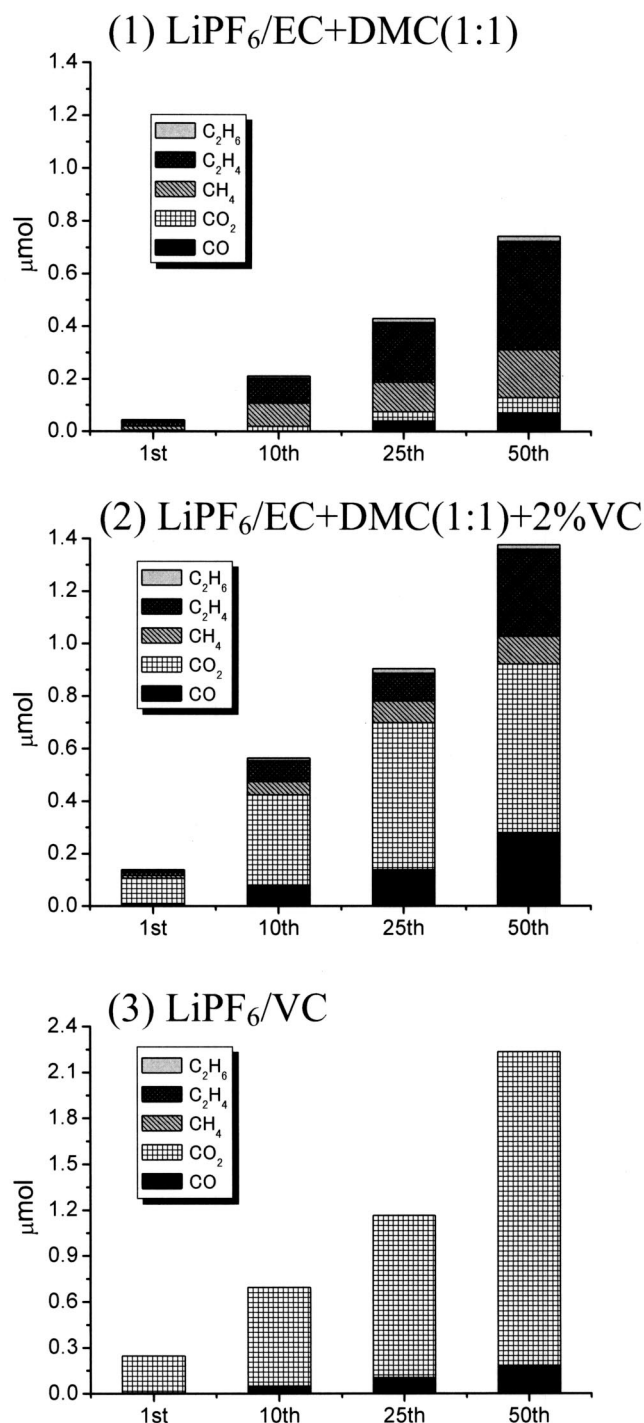


Figure 3. Evolved gas analysis during deposition and dissolution at various cycles in (1) $1 \text{ mol dm}^{-3} \text{LiPF}_6/\text{EC} + \text{DMC} (1:1)$, (2) $1 \text{ mol dm}^{-3} \text{LiPF}_6/\text{EC} + \text{DMC} (1:1) + 2 \text{ wt } \% \text{VC}$, and (3) $1 \text{ mol dm}^{-3} \text{LiPF}_6/\text{VC}$ at 25°C .

temperatures (25 and 50°C), the cycling efficiencies were typically greater than those obtained for the same reaction conducted in VC-free electrolytes. The corresponding surface films (at 25 and 50°C) obtained from reactions in both LiPF_6/VC and VC-containing $\text{LiPF}_6/\text{EC} + \text{DMC}$ electrolytes, were markedly thinner than those formed at lower temperatures and exhibited gel-like morphologies containing particulate forms, not dendrite-like morphologies. These morphologies are largely attributed to the surface film of VC-derived polymeric species. In the VC-containing electrolytes,

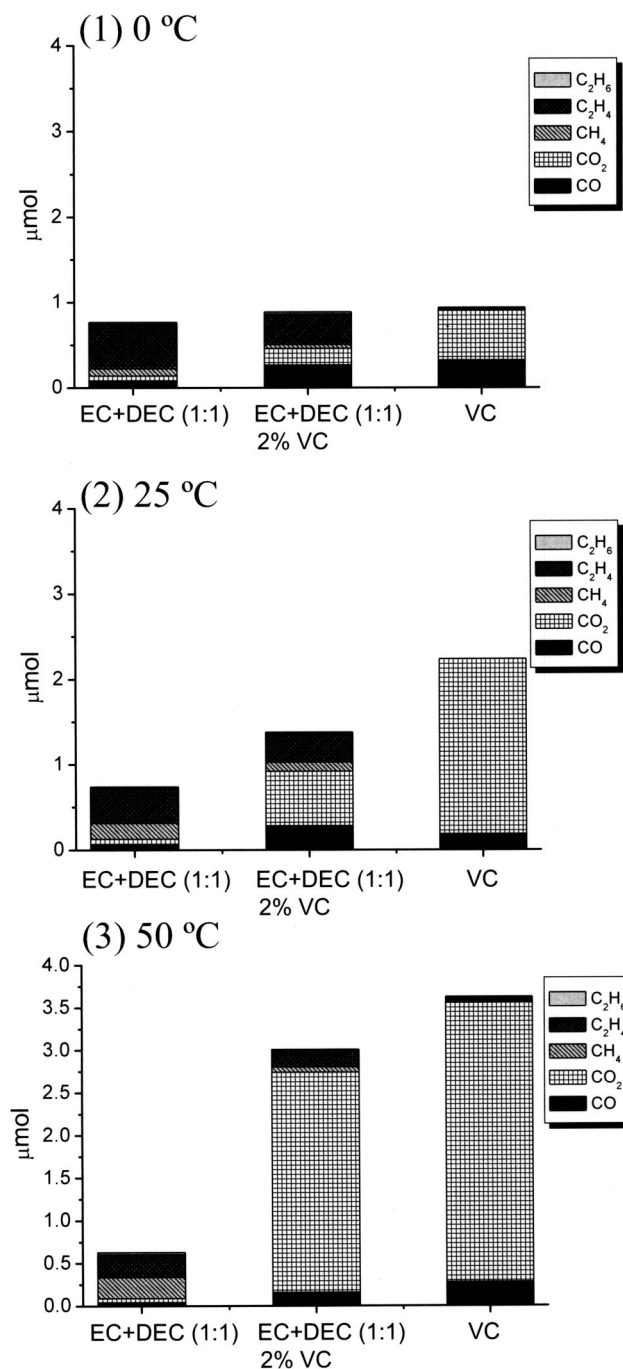


Figure 4. Evolved gas analysis after the 50th deposition and dissolution cycle in $1 \text{ mol dm}^{-3} \text{LiPF}_6/\text{EC} + \text{DMC} (1:1)$, $1 \text{ mol dm}^{-3} \text{LiPF}_6/\text{EC} + \text{DMC} (1:1) + 2 \text{ wt } \% \text{VC}$, and $1 \text{ mol dm}^{-3} \text{LiPF}_6/\text{VC}$ at various temperature: (1) 0 , (2) 25 , and (3) 50°C .

deposited lithium exhibit low reactivity with the electrolyte because gel-like morphologies become low surface areas. The surface film in the VC-containing electrolytes can prevent the deleterious reaction between deposited lithium and the electrolyte at an elevated temperature.

Evolved gas analysis during lithium deposition and dissolution.—It is common knowledge that gaseous products are generated by electrochemical side reactions between the deposited lithium and the electrolyte. The evolved gases provide important chemical information relating to the surface film formation. Figure 3 shows results

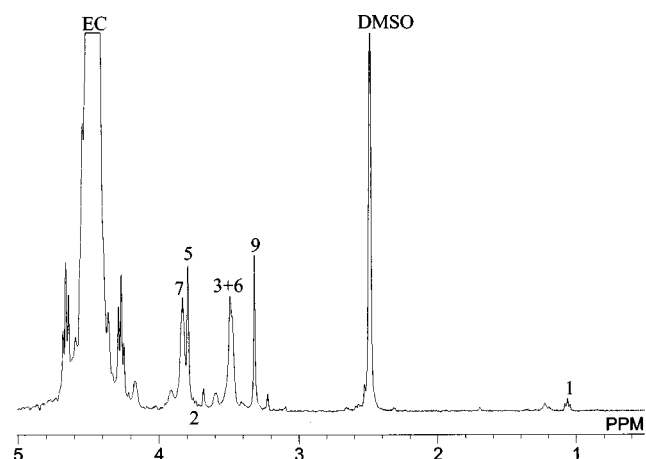


Figure 5. ^1H -NMR spectrum of dissolved solution with $\text{DMSO-}d_6$ of surface film of deposited lithium on nickel substrate in 1 mol dm^{-3} $\text{LiPF}_6/\text{EC} + \text{DMC}$ (1:1) at 25°C .

of the evolved gas analysis following lithium deposition and dissolution in a Li/Ni cell at 25°C . Electrochemical decomposition of the solvent results in the formation of ethylene (C_2H_4), carbon monoxide (CO), methane (CH_4), and carbon dioxide (CO_2), all of which were detected in the EC + DMC (1:1) electrolyte. These gas species would be related to the formation of the surface film as in the following equations³⁸



The volume of these gases was found to increase with repeated deposition and dissolution. For the lithium metal anode, the lithium cycling efficiency cannot reach 100%. Since the reaction between the deposited lithium and the electrolytes occurs with cycling, the volume of reductive gaseous species is also found to increase. When

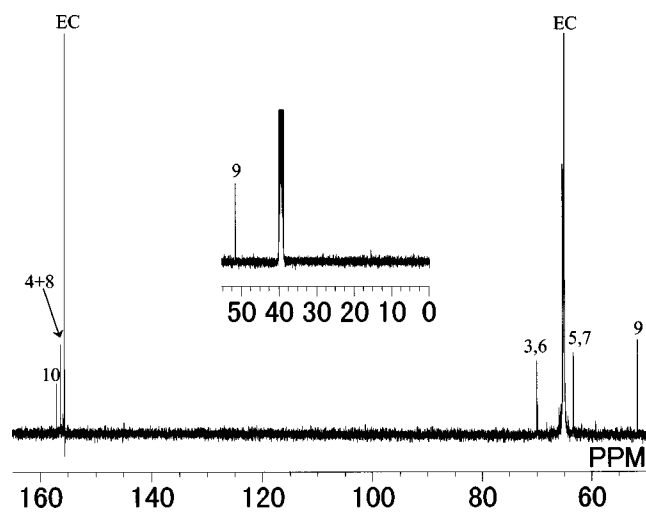


Figure 6. ^{13}C -NMR spectrum of dissolved solution with $\text{DMSO-}d_6$ of surface film of deposited lithium on nickel substrate in 1 mol dm^{-3} $\text{LiPF}_6/\text{EC} + \text{DMC}$ (1:1) at 25°C .

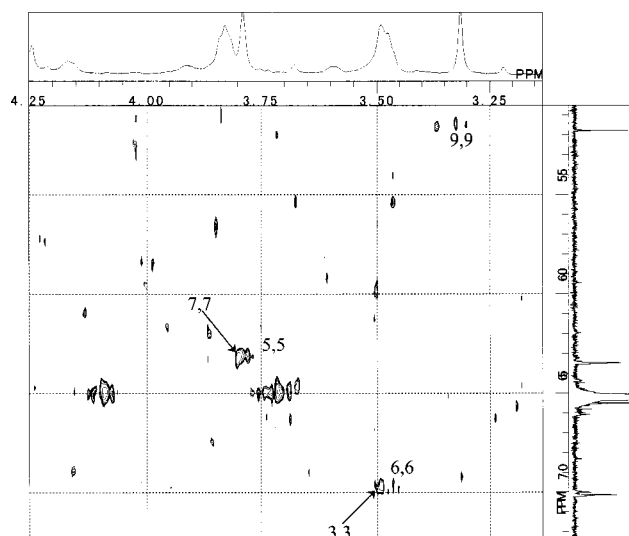


Figure 7. 2D ^1H - ^{13}C HMQC spectrum of dissolved solution with $\text{DMSO-}d_6$ of surface film of deposited lithium on nickel substrate in 1 mol dm^{-3} $\text{LiPF}_6/\text{EC} + \text{DMC}$ (1:1) at 25°C .

the anodes are substituted for graphite, the initial cycling efficiency in EC-based electrolytes is typically around 90%, the value which improves over a period of time to yield efficiencies much closer to 100%. Unlike lithium anodes, the surface films formed on graphite can prevent reductive decomposition of the electrolyte. Interestingly, the presence of VC in EC-based electrolytes was found to reduce the formation of C_2H_4 , and CH_4 , as shown in Fig. 3-2. However, the same conditions also resulted in a concomitant increase in the formation of CO_2 , with increasing cycling. These results suggest that the presence of VC decomposition products within the surface film is enough to suppress the reduction of EC-DMC. These findings are echoed in Fig. 3-3, where the LiPF_6/VC electrolyte produced a large amount of CO_2 gas and a much smaller volume of CO. Figure 4 compares the evolved gas analysis following deposition and dissolution cycling (50 times) at 0, 25, and 50°C . In the $\text{LiPF}_6/\text{EC} + \text{DMC}$ (1:1) + 2% VC and LiPF_6/VC electrolytes, the volume of CO_2 increased with increasing temperature. The volume of CO_2 formed in electrolytes containing VC additives is quantitatively larger than in VC-free electrolytes, implying that the evolution of CO_2 is directly related to the electrochemical decomposition of VC. Similarly, the lithium-graphite half-cell in the $\text{LiPF}_6/\text{EC} + \text{DMC}$ (1:1) with 2% VC and LiPF_6/VC electrolytes also generated CO_2 gas at the anode.³⁸ We conjecture that the quantity of CO_2 produced corresponds directly with the presence of VC decomposition products within the surface film.

NMR analysis of the VC-derived surface films.—The ^1H , ^{13}C , 2D (^1H - ^{13}C) HMQC (heteronuclear multiple quantum coherence) and 2D (^1H - ^{13}C) HMBC (heteronuclear multiple bond coherence) NMR spectra of the surface film of deposited lithium on nickel substrate in $\text{LiPF}_6/\text{EC} + \text{DMC}$ (1:1) are shown in Fig. 5 to 8. From the NMR results, we confirmed the presence of five components within the $\text{LiPF}_6/\text{EC} + \text{DMC}$ (1:1) electrolyte, and four components within the LiPF_6/VC electrolyte [^1H -NMR spectrum (Fig. 9) and ^{13}C -NMR spectrum (Fig. 10)]. The chemical structures of the surface films formed in both electrolyte solvent systems are shown in Fig. 11 and 12, respectively. The signals for all ^1H and ^{13}C NMR spectra have been assigned accordingly and summarized in Table I. The HMQC technique provides direct (one-bond) heteronuclear (e.g., C-H) correlations. In contrast, the HMBC technique allows the identification of proton-carbon connectivities through multiple bond couplings (typically from two to three bonds).

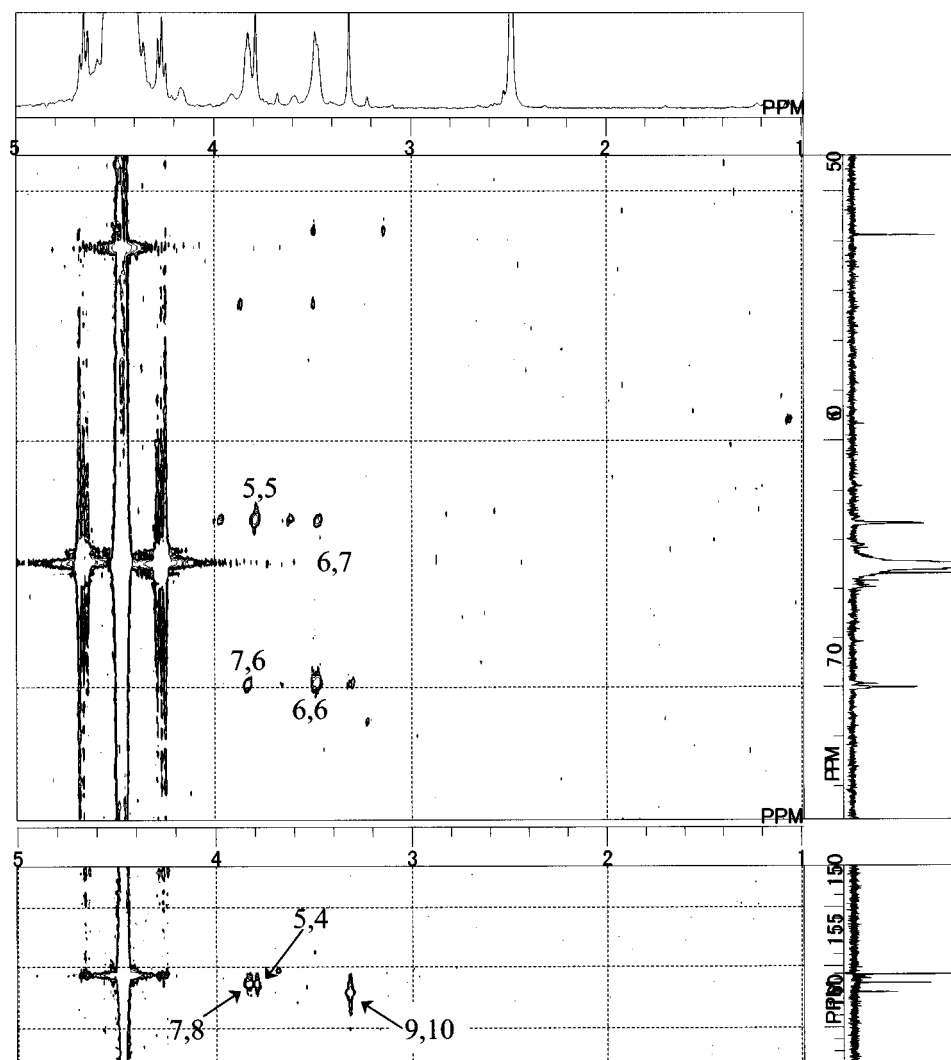


Figure 8. 2D ^1H - ^{13}C HMBC spectrum of dissolved solution with $\text{DMSO-}d_6$ of surface of deposited lithium on nickel substrate in 1 mol dm^{-3} $\text{LiPF}_6/\text{EC} + \text{DMC}$ (1:1) at 25°C .

In the ^1H NMR spectrum (Fig. 5), the triplet at 1.06 ppm and quartet at 3.77 ppm have been assigned to H-1 and H-2 in $\text{CH}_3\text{CH}_2\text{O}^-$ (compound 1), respectively. The signal at 3.50 ppm has been assigned to the methylene group $-(\text{CH}_2\text{O})-$ of polyethylene oxide (PEO, compound 2). In the HMQC spectrum (Fig. 7), the signal at 3.5 ppm, associated with H-3 $-(\text{CH}_2\text{O})-$ (compound 2), has

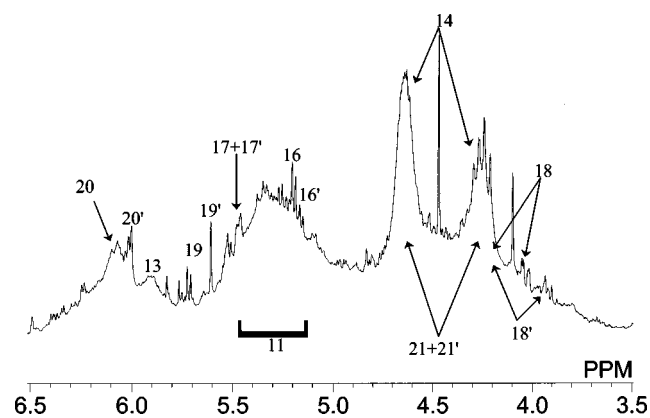


Figure 9. ^1H -NMR spectrum of dissolved solution with $\text{DMSO-}d_6$ of surface film formed of deposited lithium on nickel substrate in 1 mol dm^{-3} LiPF_6/VC at 25°C .

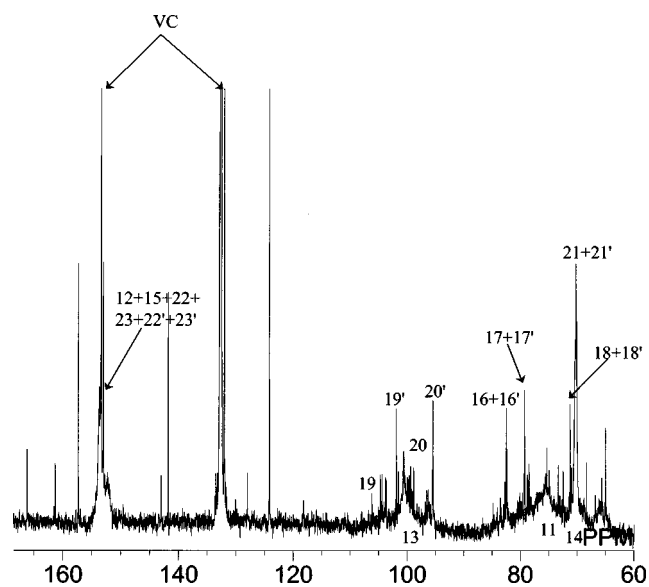


Figure 10. ^{13}C -NMR spectrum of dissolved solution with $\text{DMSO-}d_6$ of surface film formed of deposited lithium on nickel substrate in 1 mol dm^{-3} LiPF_6/VC at 25°C .

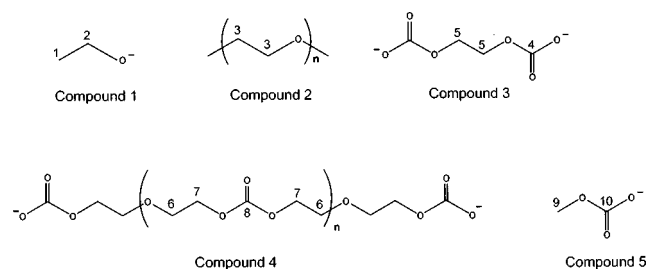


Figure 11. The structure of EC-DMC derived surface film obtained from NMR spectroscopy.

been shown to correspond with the (C-3) carbon signal at 69.9 ppm. The methylene signal at 3.8 ppm, assigned to the (H-5) proton of $(\text{CH}_2\text{OCO}_2\text{Li})_2$, (compound 3), shows a correlation with the carbon signal (C-5) at 63.4 ppm. In the HMBC spectrum (Fig. 8), the same methylene protons (H-5) are associated with the carbon (C-5) signal at 63.4 ppm, which implies that compound 3 has a contrastive structure since the CH_2 group exhibits a relationship between H-5 and C-5. Additionally, the proton (H-5) is shown to have a correlation with the carbonate carbon (C-4) at 156.4 ppm (Fig. 8). From FTIR evidence, Aurbach *et al.* proposed that $(\text{CH}_2\text{OCO}_2\text{Li})_2$ was formed following the reduction of EC.^{5,34} The NMR results support the presence of $(\text{CH}_2\text{OCO}_2\text{Li})_2$ within the surface film. In the HMQC spectrum (Fig. 7), the triplets of protons (H-6 and H-7) at 3.48 and 3.84 ppm correspond to the carbons (C-6 and C-7) at 70 and 63.4 ppm, respectively. As well as its association with (C-6) (Fig. 8), H-6 was also shown to correlate with the carbon (156.4 ppm) associated with protons H-7 and H-8. On the basis of the NMR and HMBC results, we conclude that this component (compound 4) has a carbonate-like structure with ether units within the chain (Fig. 11). C-4 and C-8 in compound 4 show the same chemical shift. Therefore, the number (n) of compound 4 may be zero for the EC + DMC electrolyte containing LiPF_6 . Compounds 1-4 were also isolated from EC + THF (1:1) electrolytes containing LiPF_6 and LiBETI following the reaction in the Li/Ni cells.³⁵ In addition, the same reaction conducted in an EC + DMC (1:1) electrolyte, generated compounds 1-4, together with a new species, lithium methyl carbonate ($\text{CH}_3\text{OCO}_2\text{Li}$) here after referred to as compound 5. Compounds 1-4 and 5 were generated following the reduction of EC and DMC, respectively. The chemical structure of compound 5 was determined using both HMQC and HMBC. In the HMQC spectrum (Fig. 8), the proton (H-9) at 3.32 ppm was found to correlate with the carbon (C-9) at 51.7 ppm. In the HMBC spectrum (Fig. 10), these same protons (H-9) were also shown to form a cross peak with the carbonate carbon (C-10) at 157.1 ppm. Compound 5 would be related to the formation of the surface film due to reductive decomposition of DMC.

Recently, our group reported on the formation of surface films on graphite anodes in LiPF_6/VC .³⁸ The present ^1H (Fig. 9) and ^{13}C -NMR (Fig. 10) results suggest the surface films of deposited

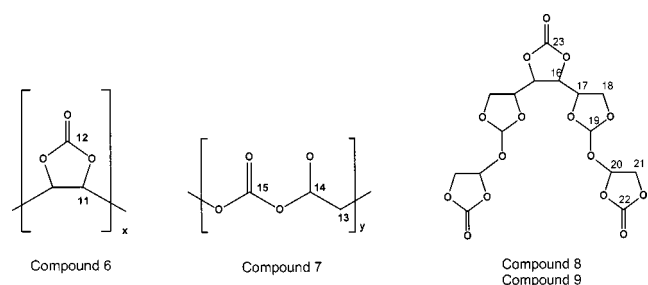


Figure 12. The structure of VC-derived surface film obtained from NMR spectroscopy.

Table I. ^{13}C NMR and ^1H chemical shifts of surface film.

	Assignment	^1H chem shift (ppm)	^{13}C chem shift (ppm)
Compound 1	1	1.1	15.50
	2	3.8	59.40
Compound 2	3	3.5	69.90
Compound 3	4		156.40
	5	3.8	63.40
Compound 4	6	3.5	70.00
	7	3.8	63.40
Compound 5	8		156.40
	9	3.3	51.70
Compound 6	10		157.10
	11	5.3	75.50
Compound 7	12		152.20
	13	5.9	100.60
Compound 8	14	4.22, 4.56	70.30
	15		153.70
Compound 9	16'	5.2	82.40
	17'	5.5	79.30
Compound 9	18'	3.96, 4.22	71.30
	19'	5.6	101.90
Compound 9	20'	6.0	95.40
	21'	4.25, 4.63	70.30
Compound 9	22'		153.70
	23'		153.70

lithium on nickel substrate in LiPF_6/VC are comparable with those previously reported on graphite. The ^1H signal (H-11) at 5.1-5.5 ppm (Fig. 9), hereafter denoted as poly-(VC), exhibits a characteristic broadness commonly associated with polymeric species. The corresponding ^{13}C signals (Fig. 10) at (C-11) 75.5 ppm and (C-12) 152.2 ppm have chemical shifts characteristic of the ring structure (compound 6) depicted in Fig. 11. The ^1H signals associated with (H-14) at 4.22 and 4.56 ppm, and the signal of (H-13) at 5.89 ppm were shown to attach directly to the carbons (C-14) at 70.3 ppm and (C-13) at 100.6 ppm in the HMQC spectrum. Based on these chemical shifts, the signals were assigned a partial structure of O-C-O. The broadening of both proton (H-13, H-14) and carbon (C-13, C-14) signals suggests compound 7 is a polymeric species, as depicted in Fig. 12. From the HMQC spectrum, the ^1H signals (H-16) at 5.19 ppm, (H-17) 5.45 ppm, (H-18) 4.03 ppm and 4.25 ppm, (H-19) 5.70 ppm, (H-20) 6.06 ppm, and (H-21) 4.25 ppm and 4.63 ppm, were found to have a close relationship with the following carbons: (C-16) at 82.5 ppm, (C-17) at 79.3 ppm, (C-18) at 71.3 ppm, (C-19) at 104.7 ppm, (C-20) at 98.8 ppm and (C-21) at 70.3 ppm. Compounds 8 and 9 have been assigned as structural isomers, since their respective ^1H and ^{13}C signals have chemical shifts that are slightly offset from those of the corresponding isomer.

It has been known that DMSO is a reactive solvent with lithium. If surface film formation between DMSO and lithium occurs, CD_3 unit in $\text{DMSO}-d_6$ would be found by ^{13}C -NMR spectra. However, a CD_3 unit related to $\text{DMSO}-d_6$ was not detected as shown in Fig. 6. This result indicates that there is no mainly DMSO-related compound. Furthermore, we confirmed the reactivity between the lithium and VC/LiPF_6 solution containing DMSO as shown in Fig. 13. Figure 13 demonstrates ^1H -NMR spectra of surface film (Fig. 13-1) in LiPF_6/VC , solution after the 50th deposition/dissolution in LiPF_6/VC (Fig. 13-2) and VC/LiPF_6 solution containing DMSO and lithium (Fig. 13-3). In ^1H -NMR spectra in Fig. 13-2 and Fig.

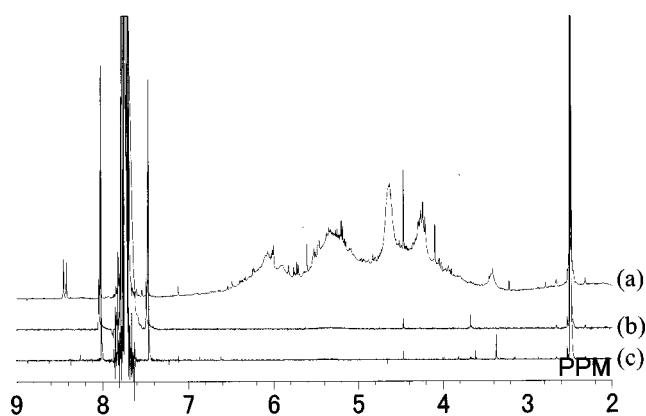


Figure 13. $^1\text{H-NMR}$ spectra of (a) surface film on nickel substrate in LiPF_6/VC , (b) solution after the 50th deposition/dissolution in LiPF_6/VC and, (c) solution after reacting lithium with DMSO in LiPF_6/VC for 24 h.

13-3, broad peaks related to the polymer could not be detected. Hence, our experiment can ignore reactions of nucleophilic surface species with DMSO. We strongly suggest that these polymers are formed by the electrochemical process, not an impurity.

GPC molecular weight determination of surface films.—Gel permeation chromatography (GPC) has been used as a chromatographic technique since the 1960s for polymer analysis, and is in common use as a fast and reliable means of gathering molecular mass distribution information. Figure 14 shows the GPC chromatograms of the surface film of deposited lithium on the nickel substrate. In typical chromatograms, very large molecules move through the column quickly (species with lower retention time) and smaller molecules are retained (species of higher retention time). When pure DMF eluents were used, sample elution occurred typically before the exclusion limit due to the presence of an ionic polymer. Consequently, all molecular weight determination analyses were conducted in DMF solutions containing 10 mM LiBr, the presence of which precluded the detection of distributions below M_w 1000. Table II shows M_n and M_w of surface film on nickel substrate by GPC, where M_n and M_w values were calculated from distributions greater than M_w 1000. The surface film formed in the $\text{LiPF}_6/\text{EC} + \text{DMC}$ (1:1) elec-

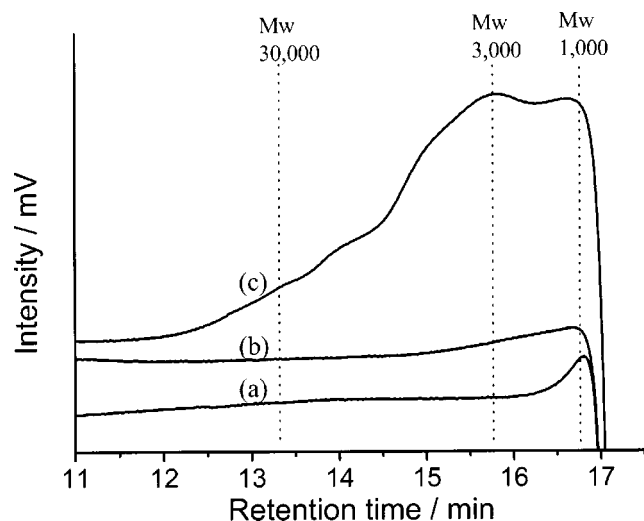


Figure 14. GPC chromatograms of the surface film of deposited lithium on nickel substrate in (a) $1 \text{ mol dm}^{-3} \text{LiPF}_6/\text{EC} + \text{DMC}$ (1:1), (b) $1 \text{ mol dm}^{-3} \text{LiPF}_6/\text{EC} + \text{DMC}$ (1:1) + 2 wt % VC, and (c) $1 \text{ mol dm}^{-3} \text{LiPF}_6/\text{VC}$ at 25°C .

Table II. The number and weight average molecular weights (M_n and M_w) of surface film on nickel substrate by GPC. (Calculated above M_w 1000.)

Electrolyte	M_n	M_w
$\text{LiPF}_6/\text{EC} + \text{DMC}$ (1:1)	1,600	1,900
$\text{LiPF}_6/\text{EC} + \text{DMC}$ (1:1) + 2% VC	2,100	2,400
LiPF_6/VC	3,100	6,700

trolyte yielded a molecular weight of M_w 1900 (Table II). This value is consistent with the formation of an oligomeric species (compound 2 and compound 4 in Fig. 11) as previously established in the NMR studies above. The dissolved solution of the surface film formed in LiPF_6/VC had a lower retention time compared to that in the VC-free electrolyte, as shown in Fig. 14(c). This result clearly indicates that the surface film contains polymeric species as shown in Fig. 12. For the surface film formed in $\text{LiPF}_6/\text{EC} + \text{DMC}$ (1:1) in the presence of 2% VC, the sample elution occurred around 14.8 min (M_w 7,500) [Fig. 14(b)]. It is sufficiently high to confirm the presence of polymers within the surface film, although the molecular weight obtained in the $\text{LiPF}_6/\text{EC} + \text{DMC}$ (1:1) + 2% VC is lower than that in the LiPF_6/VC electrolyte. The molecular weights of surface films formed in EC + DMC, EC + DMC + VC, and VC electrolytes gave M_w values of 1900, 2400, and 6700, and M_n values of 1600, 2100, and 3100, respectively, confirming that the increased VC content leads to larger molecular weights. We consider that a great part of the surface films in the EC-based electrolyte may contain relatively small molecules. The NMR spectra of surface film in the LiPF_6/VC electrolyte demonstrated polymeric species including [poly-(VC)], oligomeric VC, and a ring-opened polymer of VC. These polymers would be detected by the GPC analysis.

XPS analysis of surface films.—Figure 15 shows the C 1s and O 1s XPS spectra for the surface films of deposited lithium on a nickel substrate at 25°C , after the first dissolution step. An XPS study can obtain surface information of inorganic species in addition to organic species. For the surface film formed in the EC-DMC electrolyte, XPS confirms the existence of lithium alkyl carbonate (compound 3 in Fig. 11) with C 1s signals occurring at 291 eV (CO_3), 288 eV (CO), and 285.8 eV (CCO) in the C 1s spectrum and O 1s signals at 533.5 eV (CQC) and 532.5 eV ($\text{C}=\text{O}$). For the surface film formed in the same electrolyte containing 2% VC, XPS exhibits additional peaks within the C 1s and O 1s spectra at 534.4 and 291.8 eV, respectively, suggesting the surface film comprises poly-(VC), as well as a further C 1s signal (289 eV) corresponding to the presence of an ester ($-\text{COO}$) functionality. These peaks were also observed in the surface film formed in LiPF_6/VC . Based on the NMR results, the surface film of deposited lithium on nickel substrate in the EC-based electrolyte have been shown to comprise polymer constituents containing $-\text{CH}_2\text{O}-$ groups, which have been assigned to those of PEO (compound 2 in Fig. 11). The XPS C 1s spectrum of PEO is known to produce a peak at 286.2 eV corresponding to the $-\text{CH}_2\text{O}-$ groups.³⁵ We estimate from the C 1s spectrum in Fig. 15 that the signal at 286 eV can only be attributed to the presence of polymer constituents containing $-\text{CH}_2\text{O}-$ groups (compound 4 in Fig. 11). The additional peaks at 283.5 and 281.8 eV have been tentatively assigned to those of carbide species such as RLi and Li_2C ,^{20,21,25} that together with Li_2O , exist deep within the surface film. A comparison of the surface films measured before and after Ar^+ ion sputtering shows that the Li_2O layer formed in the VC-containing EC-DMC electrolyte (Fig. 15b) is thinner than that formed in the VC-free electrolyte (Fig. 15a). It is difficult to assign XPS spectra after Ar^+ ion sputtering, which often causes decomposition of the organic compounds within the sample. A large carbon peak at 285 eV was observed in the C 1s spectrum of the surface film formed in LiPF_6/VC , which we have tentatively assigned to

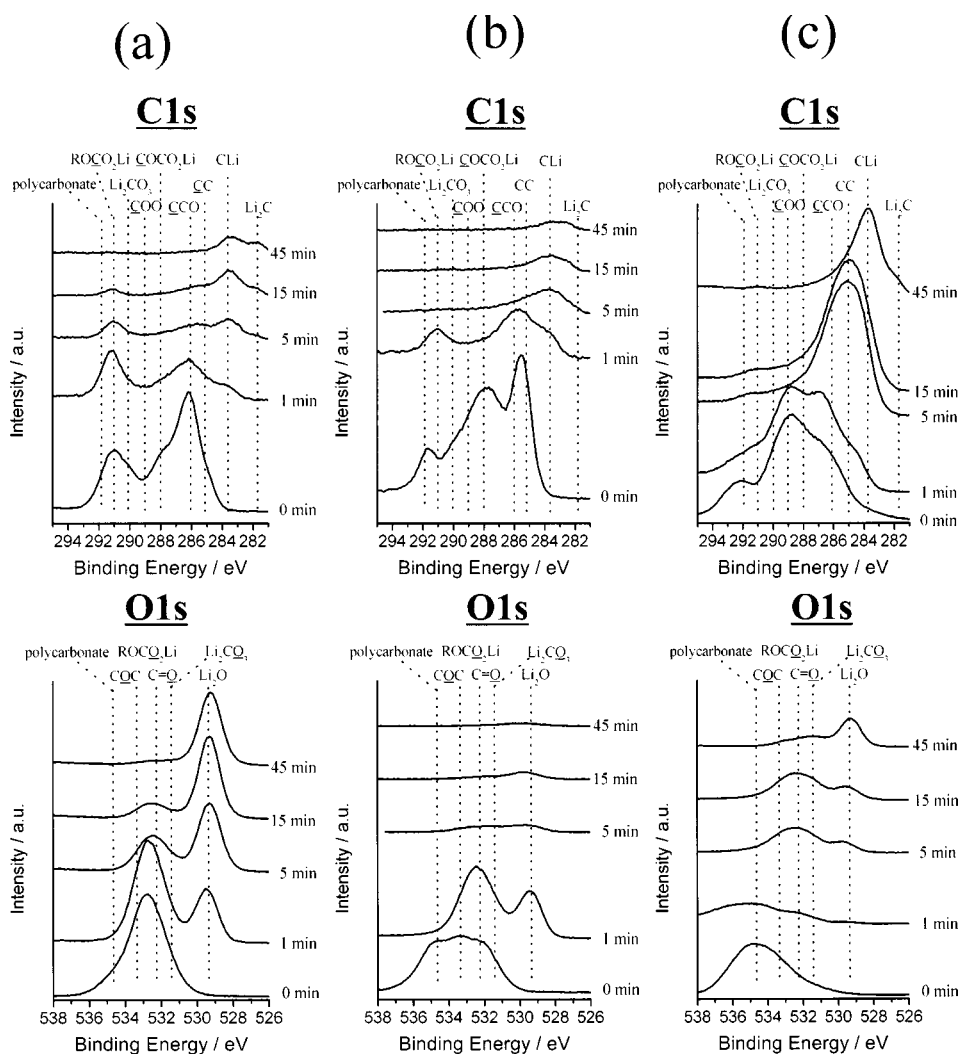


Figure 15. C 1s and O 1s XPS spectra of surface film of deposited lithium on nickel substrate in (a) $1 \text{ mol dm}^{-3} \text{ LiPF}_6/\text{EC} + \text{DMC} (1:1)$, (b) $1 \text{ mol dm}^{-3} \text{ LiPF}_6/\text{EC} + \text{DMC} (1:1) + 2 \text{ wt \% VC}$, and (c) $1 \text{ mol dm}^{-3} \text{ LiPF}_6/\text{VC}$.

polymeric and oligomeric forms of VC. The XPS measured atomic concentrations for surface films obtained before Ar^+ ion sputtering are given in Table III. The content of P (from LiPF_6) was determined to be the same for surface films formed in all electrolytes. The F (from LiF), and Li content, in the VC-derived surface films are typically lower than those detected in the VC-free surface film particularly in LiPF_6/VC , which exhibits a considerably low Li content. On the other hand, the carbon content in the VC-derived surface films is significantly higher than in the VC-free surface films. Lithium alkyl carbonate formed in EC-based electrolyte reacts with HF to form LiF . We believe that the VC-containing electrolyte suppresses the formation of LiF because VC-derived polymeric surface films are difficult to react with HF.

FTIR analysis of the VC-derived surface films.—A comparison of the FTIR spectra of surface films of deposited lithium on nickel substrate after the tenth lithium deposition-dissolution cycle at 0, 25, and 50°C , respectively, is shown in Fig. 16. The FTIR spectra of the

surface films formed in EC-based electrolytes show peaks attributed to lithium alkyl carbonate-like species (compound 3 and compound 4 in Fig. 11) [1647 cm^{-1} ($\nu_{\text{as C=O}}$), 1400 cm^{-1} ($\delta_{\text{CH}_3, \text{CH}_2}$), 1317 cm^{-1} ($\nu_{\text{s C=O}}$), 1074 cm^{-1} ($\nu_{\text{C-O}}$) and 820 cm^{-1} ($\delta_{\text{OCO}_2}^-$)]. Aurbach *et al.* assigned the peaks to be $(\text{CH}_2\text{OCO}_2\text{Li})_2$, which is the major EC reduction product on Li and Li-C electrodes.^{5,34} The FTIR spectra of the surface film formed in all electrolytes exhibited a peak at 3780 cm^{-1} , which we have assigned to the ν_{OH} stretching mode of the hydroxyl group in lithium hydroxide (LiOH). For the surface films formed in VC-containing electrolytes, FTIR spectra reveal specific peaks at 1817, 1147, 1080, and 758 cm^{-1} , which we have attributed to the presence of poly-(VC) (compound 6 in Fig. 12). The FTIR spectrum of poly-(VC), which was synthesized in order to identify poly-(VC), plotted in Fig. 16. The FTIR spectra for the surface film in the VC-containing electrolyte at 50°C correspond with the spectrum of poly-(VC). Aurbach *et al.* reported that FTIR spectrum of graphite electrodes cycled in the VC-containing electrolyte at 60°C showed the broad peak around 1850 cm^{-1} .³⁹ They assigned that the peak may belong to polycarbonate species. According to FTIR spectrum poly-(VC), it has the peak around 1820 cm^{-1} . The broad peak around 1850 cm^{-1} may be related to poly-(VC). Furthermore, the FTIR spectra of VC-derived surface films exhibit bands that are typical of a carboxylate (COOLi) functional group [1580 cm^{-1} ($\nu_{\text{CO}_2}^-$) and 1413 cm^{-1} ($\nu_{\text{CO}_2}^-$)]. In addition to poly-(VC) and RCOOLi , FTIR has also detected evidence of carbon-carbon double bonds ($\text{C}=\text{C}$) [1620 cm^{-1} ($\nu_{\text{C=C}}$) and 972 cm^{-1}

Table III. Atomic concentration of surface film by XPS.

Electrolyte	Atomic concentration (%)					
	Li	C	O	F	P	Ni
$\text{LiPF}_6/\text{EC} + \text{DMC} (1:1)$	23.9	34.2	37.9	3.8	0.2	0.0
$\text{LiPF}_6/\text{EC} + \text{DMC} (1:1) + 2\% \text{ VC}$	10.2	50.3	36.8	2.5	0.2	0.0
LiPF_6/VC	0.1	58.0	40.3	1.3	0.2	0.0

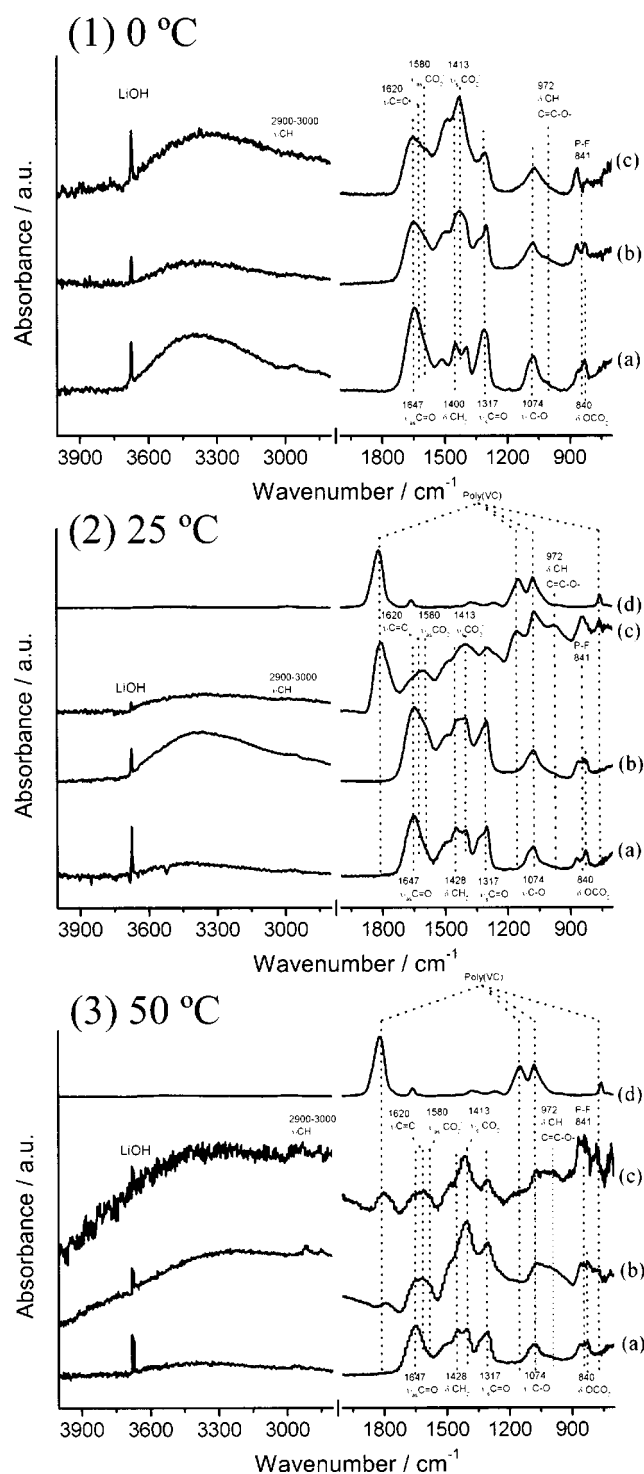


Figure 16. FTIR spectra of surface film of deposited lithium on nickel substrate in (a) $1 \text{ mol dm}^{-3} \text{ LiPF}_6/\text{EC} + \text{DMC} (1:1)$, (b) $1 \text{ mol dm}^{-3} \text{ LiPF}_6/\text{EC} + \text{DMC} (1:1) + 2 \text{ wt \% VC}$, and (c) $1 \text{ mol dm}^{-3} \text{ LiPF}_6/\text{VC}$ at various temperatures: (1) 0, (2) 25, and (3) 50°C. FTIR spectra of (d) are poly-(VC)

($\delta_{\text{C}=\text{C}-\text{O}}$) within the VC-derived surface films. Aurbach *et al.* also reported that VC is reduced to species containing $-\text{OCO}_2\text{Li}$ groups, part of which may also have C = C double bonds.³⁹ We estimate that the structure of the C = C-O unit comprises reduced VC decomposition products such as lithium vinylene dicarbonate (CHOCO_2Li)₂ and lithium divinylene dicarbonate

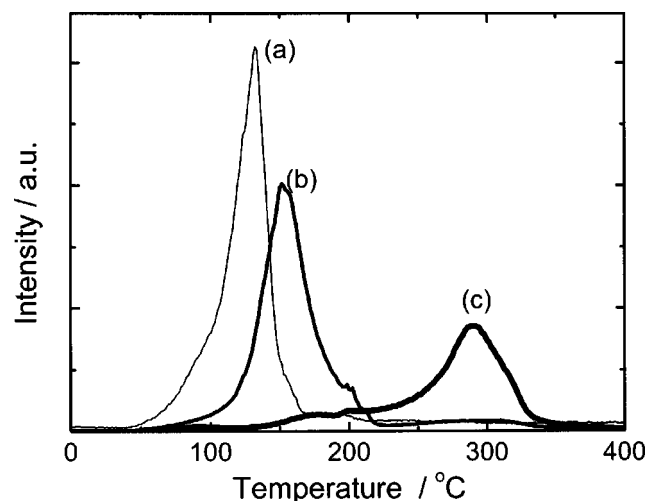


Figure 17. Thermal stability of organic surface film of deposited lithium on nickel substrate in (a) $1 \text{ mol dm}^{-3} \text{ LiPF}_6/\text{EC} + \text{DMC} (1:1)$, (b) $1 \text{ mol dm}^{-3} \text{ LiPF}_6/\text{EC} + \text{DMC} (1:1) + 2 \text{ wt \% VC}$, and (c) $1 \text{ mol dm}^{-3} \text{ LiPF}_6/\text{VC}$ at 25°C by TPD-MS.

($\text{CH} = \text{CHOCO}_2\text{Li}$)₂. These compounds were also detected in the surface film formed on graphite anodes.³⁸ The concentration of poly(VC) and C = C-O compounds within the surface film increased with increasing temperature (Fig. 16-3). According to evolved gas analysis, it was also observed that the VC-containing electrolytes generate large amounts of CO_2 at elevated temperatures, thought to be related to the formation of C = C-O functional groups. We consider that CO_2 would be related to decarbonation ($-\text{C} = \text{C}-\text{O}-$) via the reduction of VC. The reactivity between VC and deposited lithium is found to increase with increasing temperature, implying that VC-derived surface films promote effective surface film formation at elevated temperatures.

Thermal stability (TPD-MS) analysis of the VC derived surface films.—TPD-MS profiles of the surface films are shown in Fig. 17. The thermal stability of each surface film was evaluated by measuring the decomposition gas pattern of CO_2 (m/z 22) related to organic carbonate surface films. The surface film of deposited lithium on nickel substrate in the $\text{LiPF}_6/\text{EC} + \text{DMC} (1:1)$ electrolyte was shown to decompose around 130°C. While the surface films obtained from the reaction in $\text{LiPF}_6/\text{EC} + \text{DMC} (1:1) + 2\% \text{ VC}$ and LiPF_6/VC decomposed at clearly higher temperatures, 150 and 300°C, respectively. As described in the analytical results above, surface films comprising decomposed VC polymer components are found to improve the thermal stability of the organic surface film. When the thermal stability of the surface film is poor, it is also expected to occur due to the reformation of the surface film brought on by thermal decomposition at elevated temperatures. We propose, therefore, that the lithium cycling performance in the VC-containing electrolytes at elevated temperatures might be improved in surface films that exhibit high thermal stabilities.

Conclusions

We have used various analytical techniques to investigate the surface of deposited lithium on a nickel substrate in $\text{LiPF}_6/\text{EC} + \text{DMC} (1:1)$ without and with 2% VC additive and LiPF_6/VC . Moreover, the evolved gas formed during the deposition and dissolution steps has also been analyzed in order to understand its effect on surface film formation.

The presence of VC in EC-based electrolytes caused a decrease in the volume of gases (C_2H_4 and CH_4) produced due to the formation of the surface film from the EC-DMC solvent. The volume of gas produced was found to increase with repeated lithium deposition and dissolution cycling and reaction in VC-containing electrolytes at

elevated temperatures. The VC-containing electrolyte showed remarkably high lithium cycling efficiency with increasing temperature. The following conclusions can be drawn from the various analytical techniques.

Based on NMR and GPC studies, the VC-derived surface films were found to consist of the following polymeric species poly(vinylene carbonate), poly-(VC), oligomeric VC, and a ring-opened polymeric form of VC.

XPS and FTIR studies confirmed the presence of carbon-carbon double bonds (C=C-O) and carboxylate (COOLi) functional groups on the film surface.

The VC-containing LiPF₆ electrolytes suppress the formation of LiF (HF) due to the presence of polymeric VC decomposition products within the surface film.

The VC-containing electrolytes can easily form VC-derived surface films at elevated temperatures. Deleterious reactions between lithium and the electrolyte are suppressed by the presence of polymeric VC species within the surface film.

Mitsubishi Chemical Group Science and Technology Center, Incorporated, assisted in meeting the publication costs of this article.

References

- J. Yamaki and S. Tobishima, in *Handbook of Battery Materials*, J. O. Besenhard, Editor, Part III-3, Wiley-VCH, Weinheim (1999).
- K. M. Abraham, J. S. Foos, and J. L. Goldman, *J. Electrochem. Soc.*, **131**, 2197 (1984).
- S. Tobishima and T. Okada, *Electrochim. Acta*, **30**, 1715 (1985).
- M. Arakawa, S. Tobishima, T. Hirai, and J. Yamaki, *J. Electrochem. Soc.*, **133**, 1527 (1986).
- D. Aurbach, A. Zaban, Y. Gofer, O. Abramson, and M. Ben-Zion, *J. Electrochem. Soc.*, **142**, 687 (1995).
- D. Aurbach, E. Zinigrad, H. Teller, Y. Cohen, G. Salitra, H. Yamin, P. Dan, and E. Elster, *J. Electrochem. Soc.*, **149**, A1267 (2002).
- K. Naoi, M. Mori, Y. Naruoka, W. M. Lamanna, and R. Atanasoski, *J. Electrochem. Soc.*, **146**, 462 (1999).
- X. Wang, Y. Yasukawa, and S. Mori, *J. Electrochem. Soc.*, **146**, 3992 (1999).
- X. Wang, E. Yasukawa, and S. Kasuya, *J. Electrochem. Soc.*, **147**, 2421 (2000).
- Y. Sasaki, M. Handa, K. Kurashima, T. Tonuma, and K. Usami, *J. Electrochem. Soc.*, **148**, A999 (2001).
- Y. Matsuda, *J. Power Sources*, **43**, 1 (1993).
- M. Ishikawa, S. Yoshitake, M. Morita, and Y. Matsuda, *J. Electrochem. Soc.*, **141**, L159 (1994).
- M. Ishikawa, M. Morita, and Y. Matsuda, *J. Power Sources*, **68**, 501 (1997).
- K. Kanamura, S. Shiraishi, and Z. Takehara, *J. Electrochem. Soc.*, **141**, L108 (1994).
- K. Kanamura, S. Shiraishi, and Z. Takehara, *J. Electrochem. Soc.*, **143**, 2187 (1996).
- S. Shiraishi, K. Kanamura, and Z. Takehara, *Langmuir*, **13**, 3542 (1997).
- M. Morita, S. Aoki, and Y. Matsuda, *Electrochim. Acta*, **37**, 119 (1992).
- R. Mogi, M. Inaba, S.-K. Jeong, Y. Iriyama, T. Abe, and Z. Ogumi, *J. Electrochem. Soc.*, **149**, A1578 (2002).
- T. Hirai, I. Yoshimatsu, and Yamaki, *J. Electrochem. Soc.*, **141**, 2300 (1994).
- M. Mori, Y. Naruoka, K. Naoi, and D. Fauteux, *J. Electrochem. Soc.*, **145**, 2340 (1998).
- K. Naoi, M. Mori, M. Inoue, T. Wakabayashi, and K. Yamauchi, *J. Electrochem. Soc.*, **147**, 813 (2000).
- E. Plichta, S. Slane, M. Uchiyama, M. Salomon, D. Chua, W. B. Ebner, and H. W. Lin, *J. Electrochem. Soc.*, **136**, 1865 (1989).
- D. Aurbach, Y. Gofer, M. Ben-Zion, and P. Aped, *J. Electroanal. Chem.*, **339**, 451 (1992).
- J. O. Besenhard, M. W. Wagner, M. Winter, A. D. Jannakoudakis, P. D. Jannakoudakis, and E. Theodoridou, *J. Power Sources*, **44**, 413 (1993).
- T. Osaka, T. Momma, Y. Matsumoto, and Y. Uchida, *J. Electrochem. Soc.*, **144**, 1709 (1997).
- Z. Takehara, *J. Power Sources*, **68**, 82 (1997).
- C. Jehoulet, P. Biensan, J. M. Bodet, M. Broussely, C. Moteau, and C. Tessier-Lescouret, Abstract 135, p. 153, The Electrochemical Society and International Society of Electrochemistry Meeting Abstracts, Vol. 97-2, Paris, France, Aug 31-Sept 5, 1997.
- T. Hirai, I. Yoshimatsu, and J. Yamaki, *J. Electrochem. Soc.*, **141**, 611 (1994).
- M. Ishikawa, Y. Takaki, M. Morita, and Y. Matsuda, *J. Electrochem. Soc.*, **144**, L90 (1997).
- M. Ishikawa, M. Kanemoto, and M. Morita, *J. Power Sources*, **81-82**, 217 (1999).
- R. Mogi, M. Inaba, Y. Iriyama, T. Abe, and Z. Ogumi, *J. Electrochem. Soc.*, **149**, A385 (2002).
- R. Mogi, M. Inaba, Y. Iriyama, T. Abe, and Z. Ogumi, *J. Power Sources*, **108**, 163 (2002).
- H. Ota, K. Shima, M. Ue, and J. Yamaki, *Electrochim. Acta*, **49**, 565 (2004).
- D. Aurbach, *Nonaqueous Electrochemistry*, Marcel Dekker, New York (1999).
- H. Ota, Y. Sakata, X. Wang, J. Sasahara, and E. Yasukawa, *J. Electrochem. Soc.*, **151**, A437 (2004).
- H. Ota, X. Wang, and E. Yasukawa, *J. Electrochem. Soc.*, **151**, A427 (2004).
- M. Arakawa, Y. Nemoto, S. Tobishima, M. Ichimura, and J. Yamaki, *J. Power Sources*, **43-44**, 27 (1993).
- H. Ota, Y. Sakata, A. Inoue, and S. Yamaguchi, *J. Electrochem. Soc.*, **151**, A1659 (2004).
- D. Aurbach, K. Gamolsky, B. Markovsky, Y. Gofer, M. Schmidt, and U. Heider, *Electrochim. Acta*, **47**, 1423 (2002).